ELSEVIER

Tectonophysics 330 (2001) 69–92

TECTONOPHYSICS

www.elsevier.com/locate/tecto

Electrical properties of slow-spreading ridge gabbros from ODP Site 735, Southwest Indian Ridge

B. Ildefonse[a,*], P. Pezard[b,1]

[a]*Laboratoire de Tectonophysique, ISTEEM, CNRS UMR5568, Université Montpellier II, 34095 Montpellier cedex 5, France*
[b]*Cerege (CNRS), BP80, 13545 Aix-en-Provence cedex 4, France*

Received 28 March 2000; accepted 25 September 2000

Abstract

ODP hole 735B (ODP Legs 118 and 176) samples a block of igneous crust which was accreted at the ultraslow-spreading Southwest Indian Ridge, and was uplifted to seafloor by progressive unroofing along a north-dipping low-angle detachment fault. Physical properties of a set of gabbroic samples from ODP Hole 735B have been measured in the laboratory, with a particular emphasis on the analysis of electrical properties. The electrical formation factor (F) and surface conductivity (C_s) are calculated using the model of Revil and Glover [Geophys. Res. Lett., 25 (1998) 691], from measurements at room pressure, and different salinities of the saturating fluid. The acoustic compressional velocities are in the same range as those previously measured on ODP Leg 118 samples [Proc. ODP, Sci. Results, 118 (1991) 227]. The porosity (ϕ) is low ($<1\%$) in most, fresh samples. The analysis of the porosity structure, characterised by the electrical tortuosity (τ) and the electrical cementation factor (m), reveals that the cored gabbro section is segmented in two parts. The upper part (approximately the upper half) has a nearly constant τ of 15, independent of the degree of alteration of the sample, indicating that the porous network is controlled by primary microstructures, such as grain boundaries, and by extension plastic foliations. Modifications with time and alteration are restricted to increases of ϕ and m, i.e. a higher variability of the channel thicknesses. In the lower part of the hole, fresh rocks predominate, and the porosity structure is different, with variable τ (3–10), very low m ($1.4 \pm$ SEM) and low ϕ ($0.8 \pm$ SEM%). This indicates a simpler porous network compared to that at shallower depths, probably dominated by well aligned cracks. The change in porosity structure downhole may be explained several ways, and may integrate the whole history of the crustal section cored at ODP site 735 since accretion, including plastic deformation related to unroofing of the lower crust gabbros along a low-angle detachment fault, cooling, and alteration due to hydrothermal flow at various temperatures. The electrical conduction via electronic processes in metallic minerals is not taken into account in our analysis of the electrical properties; we propose a new constitutive law for electrical conduction, that would account for the conductive mineral matrix.

Keywords: ODP site 735; physical properties; southwest Indian Ridge; hydrothermal alteration; electrical properties; oceanic crust

1. Introduction

Our knowledge of the in-situ structure of mid-ocean ridges and oceanic crust is based on geological (e.g. Dick et al., 1991) and geophysical investigations (e.g. The MELT Seismic Team, 1998), or downhole measurements (e.g. Goldberg, 1997). The analysis of

* Corresponding author. Fax: +33-0-467-143-818.
E-mail address: benoit@dstu.univ-montp2.fr (B. Ildefonse).
[1] Present address: Laboratoire de Tectonophysique, ISTEEM, CNRS UMR5568, Université Montpellier II, 34095 Montpellier cedex 5, France.

0040-1951/00/$ - see front matter
PII: S0040-1951(00)00220-1

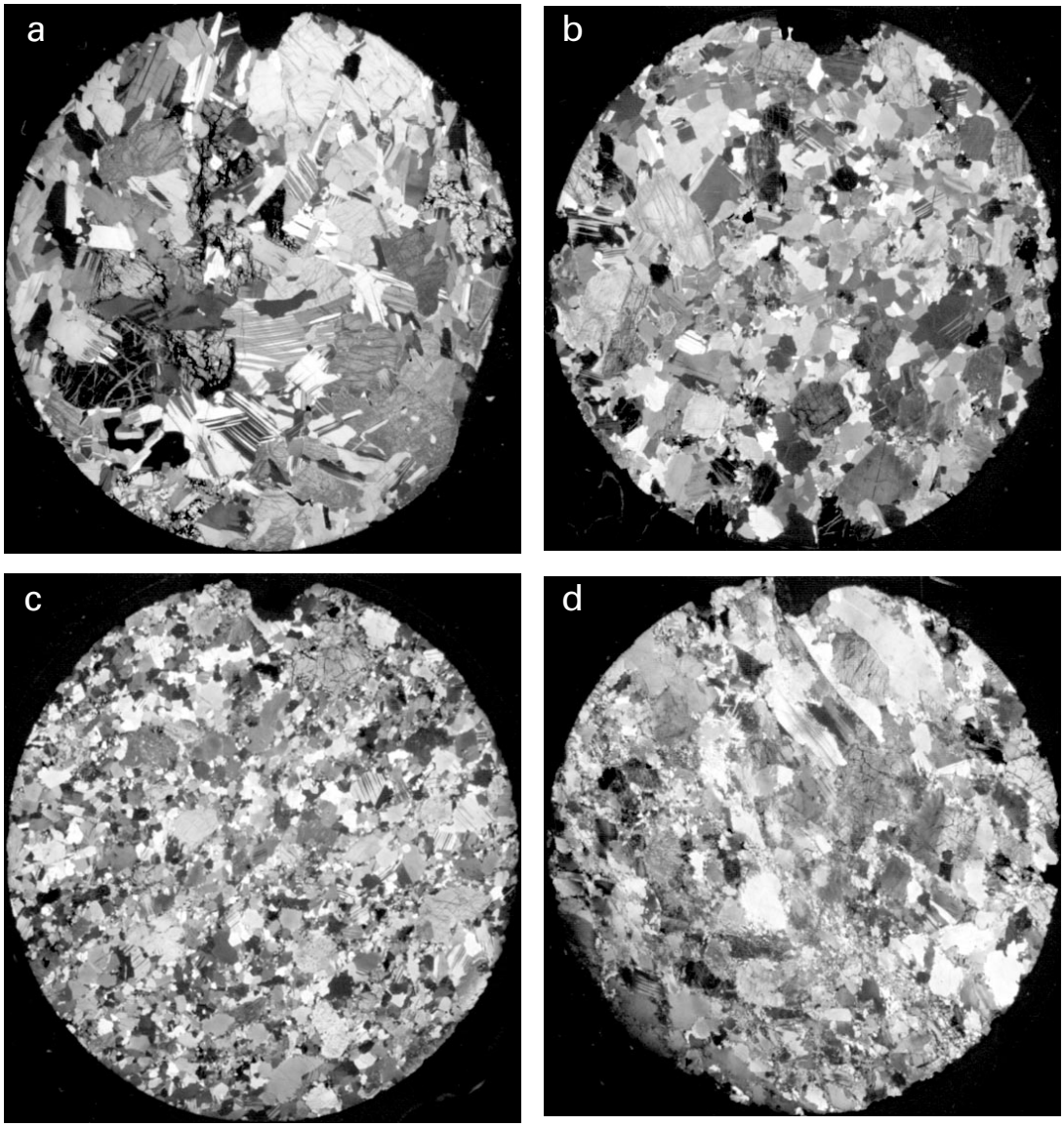

Fig. 1. Photomicrographs of 4 mini-core thin sections (cross-polarised light) in four distinct type of macroscopic structures (Table 1). (a) 176-735B-209-7-100/102; Coarse-grained igneous texture, no magmatic foliation, no or very weak plastic deformation. (b) 176-735B-154-5-42/44; Weak, high-temperature, plastic deformation overprinting a moderate magmatic shape preferred orientation. Note the equilibration of the texture, with grain-boundary migration, compared with (a). (c) 176-735B-133-3-0/7; High-temperature (sub-solidus or granulite facies) plastic foliation, with abundant recrystallisation of plagioclase (grain-boundary migration and subgrain rotation), moderate recrystallisation of olivine (subgrain rotation), and no deformation of clinopyroxene. (d) 176-735B-116-4-127/129; Low temperature (amphibolite facies) plastic foliation, with abundant recrystallisation and strong grain-size reduction of plagioclase and olivine.

marine geophysical data requires a complete understanding of the intrinsic physical properties of investigated section. For this purpose, laboratory measurements (e.g. Iturrino et al., 1991; Pezard et al., 1991; Iturrino et al., 1996) of oceanic samples physical properties provide direct insights into the physical structure and evolution of the oceanic crust.

In this paper, we present a petrophysical study of

gabbroic samples from ODP Site 735, on the Atlantis bank, near the ultraslow-spreading Southwest Indian Ridge (SWIR). The physical properties are investigated at room pressure and temperature in order to characterise in a relative sense the penetrated massif, as well as to determine the influence of alteration due to fluid circulation on host rock properties. Porosity, density, electrical properties (formation factor, surface conductivity and electrical tortuosity), bulk magnetic susceptibility and compressional velocity have been measured on a set of 34 samples collected during ODP Leg 176. Our analysis also includes a series of 29 previously studied samples from the upper part of the hole (Pezard et al., 1991). As transport properties of low-permeability rocks are still not well understood, this paper focuses on the study of electrical properties. Due to an extreme sensitivity and in spite of complexity, electrical methods are among the most precise indirect tools for multi-scale analyses of rock structures. At low frequencies ($<$1 kHz), electrical properties of saturated rocks are influenced by the mineralogical nature of the rock matrix, the chemical composition and salinity of the saturating fluid, the cation exchange processes along pore surfaces, and the topology of the porous space (e.g. Waxman and Smits, 1968; Olhoeft, 1981; Walsh and Brace, 1984; Pape et al., 1985; Katsube and Hume, 1987; Pezard, 1990; Pezard et al., 1991; Revil et al., 1998).

The main objectives of this study are i) to identify possible downhole changes in electrical properties, ii) to analyse the relationships of electrical properties with the porosity structure and alteration of the penetrated gabbroic massif, and iii) to discuss the possible constraints brought by our data on the geodynamics of the Atlantis bank.

2. Geological setting

ODP Hole 735B is located at 32°43′S–57°17′E, on top of a shallow bank (720 m below sea level), about 18 km east of the active Atlantis transform fault. It samples a block of igneous crust which was accreted about 11.5 My ago at the SWIR (Shipboard Scientific party, 1999a; Fig. 1). The SWIR has the peculiarity to be one of the slowest spreading sections of the mid-ocean ridge system, with a full spreading rate of 16 mm/yr (Fisher and Sclater, 1983). The Atlantis bank consists mostly of outcropping gabbros (MacLeod et al., 1998), and is interpreted as the result of progressive unroofing along a north-dipping low-angle detachment fault (e.g. Cannat et al., 1991; Hirth et al., 2000), in a tectonic situation similar to that of the inside-corner highs of the Mid-Atlantic Ridge (e.g. Tucholke et al., 1998).

The first 500 m of ODP hole 735B were drilled at the end of 1987, during ODP Leg 118 (Von Herzen et al., 1991). Ten years later, it was deepened to 1508 meters below sea-floor (mbsf) during ODP Leg 176 (Shipboard Scientific party, 1999a). The exceptionally high bulk core recovery of 86.5% makes the rocks of ODP hole 735B a unique, quasi-continuous, sample of the in-situ gabbroic crust. So far, the latter has been studied in shallower drilling holes located near the East Pacific Rise (Leg 147 at Hess Deep, Mével et al., 1996) and the Mid-Atlantic Ridge (Leg 153 at Mark Area, Karson et al., 1997).

The lithostratigraphy of ODP hole 735B is presented in detail in Dick et al. (1991) for the ODP Leg 118 cores and in Shipboard Scientific party (1999b) and Dick et al. (2000) for the Leg 176 cores. Gabbroic rocks constitute more than 99 vol% of the total section (Shipboard Scientific party, 1999a). This section is made of five principle gabbroic units, and more secondary intrusive units, a number of them being late small ferro–gabbro intrusions. The igneous stratigraphy is primarily controlled by the interconnection between deformation, magma segregation and crystallisation, rather than in-situ upward differentiation of magma bodies (Shipboard Scientific party, 1999a; Dick et al., 2000). ODP Hole 735B gabbroic rocks preserve a complex record of high-temperature metamorphism, brittle failure, and hydro-thermal alteration that began at near-solidus temperatures and continued down to zeolite facies metamorphic conditions. Secondary mineral assemblages in the Leg 176 core are broadly similar to those located higher up in the sequence (Stakes et al., 1991). Rocks deeper in the section are, however, remarkably fresh over large sections of the core, with extensive intervals ($>$300 m) marked by less than 10% total background alteration (Shipboard Scientific party, 1999b). There is a considerable variation in the structures observed throughout ODP hole 735B, both in style and location. The deformation structures and

microstructures account for a large range of deformation conditions, from magmatic and hypersolidus flow, to low-temperature semi-brittle and cataclastic deformation (Shipboard Scientific party, 1999b).

3. Sample description

This study comprises a series of samples from ODP Leg 176, and re-uses data from a set of ODP Leg 118 samples (Pezard et al., 1991; Table 1). The ODP Leg 176 samples are shared with another ODP Leg 176 participant (G. Iturrino) in an attempt to generate an integrated set of petrophysical data from a single set of samples (Iturrino et al., in prep.). This set includes mini-cores (25 mm in diameter, 18–50 mm long) drilled vertically (V in Table 1) and horizontally (parallel to the cut face, H in Table 1) into the core before splitting it into working and archive halves. It was completed by the closest shipboard mini-core, in the horizontal direction, perpendicular to the cut face (H′ in Table 1), sampled on-board ship for physical property and paleomagnetic measurements. This set of 11 groups of orthogonal samples from the lower section of the hole (ODP Leg 176) was measured for intrinsic properties and anisotropy of the investigated properties in the core reference frame. However, in some sample groups, the third, horizontal (H′) mini-core was unfortunately not always taken from the same interval as V and H mini-cores (Table 1). This may result locally in a different lithology and/or microstructure (i.e. samples 176-735B-116). Therefore, the anisotropy of V_p and electrical properties was calculated in two dimensions only, from measurements on mini-cores V and H. The primary criterion for choosing the sampled intervals on-board ship was the freshness of the core. It results in a rather homogeneous sampling, without strongly altered or Fe–Ti oxide-rich samples (except for 176-735B-96-2-54/58). However, the Leg 176 samples are variously deformed, with some of them containing magmatic and/or plastic foliations (Table 1; Fig. 1).

The measurements from Pezard et al. (1991) are used here to compute a set of petrophysical parameters on the basis of a new theoretical model for surface electrical conduction (Revil and Glover, 1998; see discussion below). This set of samples from ODP Leg 118 was sent back to the ODP core repository after the original study then, later, unfortunately lost. Therefore, the only available data related to these samples are that provided in Pezard et al. (1991).

4. Background

The sensitivity of electrical properties of porous media to fluid content and alteration provides a powerful means to detect conductive horizons such as fractures, either open or mineralised, in a resistive matrix (e.g. Walsh and Brace, 1984; Katsube and Hume, 1987; Pezard and Luthi, 1988). At a metre-scale, in situ measurements of electrical resistivity have historically been analysed to derive porosity (Archie, 1942; Brace et al., 1965; Becker, 1985). The different modes by which the electrical current is being transported may be identified in the laboratory, providing, with the analysis of surface electrical conduction (Waxman and Smits, 1968; Pezard, 1990; Revil and Glover, 1998), insights into the degree of alteration of the rock. The method used herein was initially derived for porous media such as sandstones and clays (Waxman and Smits, 1968; Revil and Glover, 1998). Nevertheless it has been used successfully in various low-porosity/permeability rocks, such as basalts (Pezard, 1990; Einaudi et al., 2001), gabbros (Pezard et al., 1991; Ildefonse et al., 1999), peridotites (Ildefonse et al., 1999; Ildefonse et al., 2000), and granites (Pape et al., 1985; Pezard et al., 1999; Pezard et al., 2000). However, the presence of numerous Fe–Ti oxide-rich levels in ODP Hole 735B (Natland et al., 1991; Shipboard Scientific party, 1999a) leads to a more complex conduction mechanism for the transport of electrical charges in the rock. Matrix conduction mechanisms via electronic processes in metallic oxide grains becomes then significant (Drury and Hyndman, 1979; Pezard, 1990; Pezard et al., 1991). This mineral-supported conduction mechanism constitutes a limitation to the proposed method for some samples, mostly from ODP Leg 118. One of the objectives of this paper is to propose a more complete constitutive law for electrical conduction including a potential contribution from the mineral phase. In the absence of oxide-rich gabbros, the electrical conductivity in the studied samples remains as

discussed below a combination of pore volume and pore surface conduction.

4.1. Electrical conductivity

In a porous media comprising a matrix considered as infinitely resistive and a connected pore space saturated with a conductive electrolyte, two main mechanisms are responsible for electrical conduction: (1) an electrolytic conduction mechanism in pore volumes; and (2) a surface conduction mechanism at the interface between the electrolyte and minerals. While the former is directly related to the nature and salinity of the pore fluid, the latter is due to the presence along pore surfaces of charges which are necessary to guarantee the bulk electroneutrality of the medium. In most geological settings (mineralogies and fluid pH), the mineral surfaces are charged negatively. The cations present in the fluid along pore surfaces migrate through a so-called diffuse layer to contribute to the overall conduction (e.g. Revil and Glover, 1998).

When the surface conduction component is negligible with respect to the electrolytic component (as in the case of a pure quartz sand for instance), the total conductivity of the pore space (C_o) can be considered as directly proportional to that of the saturating fluid (C_w). The proportionality coefficient $1/F$ is dimensionless and the inverse of the electrical "formation factor" F, with:

$$C_o = \frac{C_w}{F}. \tag{1}$$

The formation factor, F has often been considered to characterise the 3D topology of the pore space (e.g. Guéguen and Palciauskas, 1992).

When surface processes cannot be neglected with respect to electrolytic conduction, which is generally the case in the presence of alteration phases or clays, Eq. (1) no longer holds. Waxman and Smits (1968) proposed an empirical model to take into account the excess conductivity (C_s) due to surface processes, with:

$$C_o = \frac{C_w}{F} + C_s. \tag{2}$$

The surface conductivity C_s has been related to the notion of cation exchange capacity (*CEC*) of the altered phase in the pore space (Waxman and Smits, 1968). The *CEC* represents the number of cations that might be adsorbed per unit weight of rock matrix powder ground to 150 μm, and is expressed in meq/100 g (or in cmol/kg). Normalised per unit volume, the *CEC* is often noted Q_v and expressed in meq/ml, with:

$$Q_v = CEC\rho_m \frac{(1-\phi)}{\phi}, \tag{3}$$

where ρ_m is the matrix grain density, and ϕ the porosity. The electrical conductivity of the pore space may then be written (Waxman and Smits, 1968):

$$C_o = \frac{C_w + \dfrac{BQ_v}{\mu^2}}{F}, \tag{4}$$

where B represents the mobility of the cations in the diffuse layer, and μ^2 represents the added tortuosity of pore surfaces with respect to pore volumes. This model is still considered as satisfactory at high fluid salinity (HS), but poor at low fluid salinity (LS), with a tendency to overestimate surface conductivity processes as revealed by laboratory measurements. While the Waxman & Smits (WS) model is based on a constant Q_v value, B is considered to decrease while, in fact, the cation mobility tends to increase at low salinity due to a decrease of the ionic strength of the solution. A new and non-empirical approach based on the pore space microgeometry has been proposed by Revil and Glover (1998), with:

$$C_o = \frac{C_w}{F}[1 - t^f_{(+)} + F\xi + f(F,\xi)] \tag{5}$$

where $t^f_{(+)}$ is the Hittorf number of cations in the electrolyte (Revil and Glover, 1997), and ξ is the dimensionless parameter defined by Kan and Sen (1987), where:

$$\xi = \frac{C_s}{C_w} \approx \frac{2}{3}\frac{\phi}{1-\phi}\frac{\beta_s Q_v}{C_w} = \frac{2}{3}\frac{\beta_s \rho_m CEC}{C_w} \tag{6}$$

and β_s is the ionic mobility determined by Revil & Glover (RG) from a database including 129 samples with different types of clay (Revil and Glover, 1998). For a monovalent solute with Na^+ ions, RG propose $\beta_s = 5.14 \times 10^{-9}\ m^2\ s^{-1}\ V^{-1}$ at 25°C, and $t^f_{(+)}(Na^+) \approx 0.38$. The parameter *f(F, ξ)* is a complex function of F and ξ detailed by RG. The predictive

Table 1
Sample identification and shipboard macroscopic observations. *Mf* and *Pf* are intensities of magmatic and plastic foliations, respectively (*Mf* 2 = moderate shape fabric; *Pf* 2 = strongly foliated). V, H, H′ stand for vertical, horizontal parallel to core cut face, and horizontal perpendicular to core cut face, respectively

Sample ID	Lithologic unit (118) Igneous interval (176)	Sample type (118) Lithology (176)	Depth (mbsf)	Plagioclase (%)	Augite (%)	Olivine (%)	Opx/Pig (%)	Opaques (%)	Background alteration (%)	*Mf* intensity	*Mf* dip	*Pf* intensity	*Pf* dip
118-735B-06-1	I	Fresh	20										
118-735B-12-1	I	Tectonised	40										
118-735B-14-2	II	Tectonised	52.47										
118-735B-22-4	II	Tectonised	98.87										
118-735B-30-5	II	Fresh	142.98										
118-735B-31-3	II	Fresh	146.43										
118-735B-32-4	II	Tectonised	152.31										
118-735B-40-1	III	Fresh	191.45										
118-735B-41-4	III	Fresh	201.36										
118-735B-47-3	IV	Fresh	225										
118-735B-48-1	IV	Fe–Ti oxide-rich	231.93										
118-735B-50-4	IV	Fe–Ti oxide-rich	242.81										
118-735B-53-2	IV	Fe–Ti oxide-rich	254.86										
118-735B-53-4	IV	Tectonised	257.83										
118-735B-56-2	V	Fe–Ti oxide-rich	272.37										
118-735B-57-4	V	Tectonised	279.59										
118-735B-58-2	V	Fresh	281.96										
118-735B-61-4	V	Fresh	300.77										
118-735B-63-1	V	Tectonised	306.43										
118-735B-72-5	V	Fresh	363.86										
118-735B-73-5	V	Fresh	371.41										
118-735B-77-3	VI	Fresh	407.83										
118-735B-78-2	VI	Tectonised	411.68										
118-735B-79-5	VI	Fe–Ti oxide-rich	420.48										
118-735B-80-7	VI	Fe–Ti oxide-rich	432.85										
118-735B-85-5	VI	Tectonised	477.76										
118-735B-86-5	VI	Fresh	488.25										
118-735B-86-6	VI	Fresh	488.43										
118-735B-87-1	VI	Fe–Ti oxide-rich	491.38										

Table 1 (*continued*)

Sample ID	Lithologic unit (118) Igneous interval (176)	Sample type (118) Lithology (176)	Depth (mbsf)	Plagioclase (%)	Augite (%)	Olivine (%)	Opx/Pig (%)	Opaques (%)	Background alteration (%)	*Mf* intensity	*Mf* dip	*Pf* intensity	*Pf* dip
176-735B-96-2-49/51 (H′)	524	Opx-bearing oxide gabbro	550.29	55	40	2	2	3	5–15	1	0	1	
176-735B-96-2-54/58 (V)	524	Opx-bearing oxide gabbro	550.34	55	40	2	2	3	5–15	1	0	1	
176-735B-116-4-127/129 (H)	573	Opx-bearing gabbro	677.04	50	35	3	3	0.7	18	1	42	1	39
176-735B-116-4-129/133 (V)	573	Opx-bearing gabbro	677.06	50	35	3	3	0.7	18	1	42	1	39
176-735B-116-5-7/9 (H′)	575	Gabbronorite	677.27	55	35	1	7	0.8	10	1	46	2	37
176-735B-133-2-126/128 (H′)	662	Olivine gabbro	825.5	65	35	6	–	0.5	40	1	36	2	
176-735B-133-3-0/7 (V)	662	olivine gabbro	825.63	65	35	6	–	0.5	~60	0		2	45
176-735B-133-3-7/9 (H)	662	olivine gabbro	825.7	65	35	6	–	0.5	~60	0		2	45
176-735B-142-3-86/88 (H′)	693	olivine gabbro	896.47	65	35	8	–	0.5	10	0		1	
176-735B-142-5-0/6 (V)	693	Olivine gabbro	898.44	65	35	8	–	0.5	12	2	36	1	45
176-735B-142-5-6/8 (H)	693	Olivine gabbro	898.5	65	35	8	–	0.5	12	2	36	1	45
176-735B-147-6-32/39 (V)	710	Gabbro	947.26	55	30	2	–	0.6	40	0		2	52
176-735B-147-6-39/41 (H)	710	Gabbro	947.33	55	30	2	–	0.6	40	0		2	52
176-735B-147-6-43/45 (H′)	710	Gabbro	947.37	55	30	2	–	0.6	40	0		2	52
176-735B-147-6-55/57 (H′)	710	Gabbro	947.49	55	30	2	–	0.6	40	0		2	52
176-735B-154-5-32/34 (H′)	731	Olivine gabbro	1010.59	65	35	8	–	0.5	8	2	48	1	50
176-735B-154-5-42/44 (H)	731	Olivine gabbro	1010.69	65	35	8	–	0.5	8	2	48	1	50
176-735B-154-5-44/50 (V)	731	Olivine gabbro	1010.71	65	35	8	–	0.5	8	2	48	1	50
176-735B-158-4-65/67 (H′)	768	Olivine gabbro	1048.63	55	35	6	–	0.5	6	2	41	1	45
176-735B-158-4-80/84 (V)	768	Olivine gabbro	1048.78	55	35	6	–	0.5	6	0		0	
176-735B-158-4-84/86 (H)	768	Olivine gabbro	1048.82	55	35	6	–	0.5	6	0		0	
176-735B-166-1-21/23 (H′)	812	Gabbro	1111.11	60	30	1	–	0.5	2	1	32	0	
176-735B-167-6-103/107 (V)	812	Gabbro	1128.28	60	30	1	–	0.5	2	1	26	0	
176-735B-167-6-109/112 (H)	812	Gabbro	1128.34	60	30	1	–	0.5	2	1	26	0	
176-735B-168-2-10/12 (H′)	812	Gabbro	1131.49	60	30	1	–	0.5	3	0		0	
176-735B-179-5-90/97 (V)	845	Olivine gabbro	1227.35	55	25	20	–	0.5	2	0		0	
176-735B-179-5-97/99 (H)	845	Olivine gabbro	1227.42	55	25	20	–	0.5	2	0		0	
176-735B-179-5-110/112 (H′)	845	Olivine gabbro	1227.55	55	25	20	–	0.5	2	0		0	
176-735B-190-4-67/69 (H′)	890	Troctolitic gabbro	1330.9	65	15	12	–	0.7	5	1(2)	45	1	50
176-735B-190-4-80/86 (V)	890	Troctolitic gabbro	1331.03	65	15	12	–	0.7	5	1(2)	45	1	50
176-735B-190-4-87/89 (H)	890	Troctolitic gabbro	1331.1	65	15	12	–	0.7	5	1(2)	45	1	50
176-735B-209-7-97/99 (H′)	952	Olivine gabbro	1497.16	60	30	10	–	–	3	0		0	
176-735B-209-7-100/102 (H)	952	Olivine gabbro	1497.19	60	30	10	–	–	3	0		0	
176-735B-209-7-102/108 (V)	952	Olivine gabbro	1497.21	60	30	10	-	-	3	0		0	

capacity of this model covers the practically useful salinity range. While WS propose:

$$\left.\begin{aligned} C_o &= \frac{C_w}{F}[1 + F\xi] \quad \text{(HS)},\\ C_o &= \xi C_w \qquad\quad \text{(LS)}, \end{aligned}\right\}, \tag{7}$$

the use of the RG model is more precise, yielding the following high and low salinity end-members:

$$\left.\begin{aligned} C_o &= \frac{C_w}{F}[1 + 2\xi(F-1)] \quad \text{(HS)},\\ C_o &= \xi C_w\left[1 - \frac{(\xi-1)}{\xi F}\right] \quad \text{(LS)}. \end{aligned}\right\}. \tag{8}$$

4.2. Porosity structure

In the absence of clay or alteration phases, the electrical formation factor F, Eq. (1) depends primarily on porosity and structure. The surface conductivity C_s is then negligible when compared to the fluid conductivity C_w. The formation factor F is measured or modelled to increase as the porosity decreases or the conduction path becomes more tortuous. An empirical relationship between the electrical formation factor F and porosity ϕ was proposed by Archie (1942) with:

$$F = \phi^{-m}, \tag{9}$$

and m considered as a constant generally comprised between 1.5 and 2.5 (e.g. Guéguen and Palciauskas, 1992) for a given rock, and called the electrical cementation factor.

This relationship may also by expressed in terms of degree of connectivity of the inner pore space, or the inverse with electrical tortuosity τ (Walsh and Brace, 1984; Pezard, 1990; Pezard et al., 1991; Guéguen and Palciauskas, 1992), yielding:

$$F = \frac{\tau}{\phi}. \tag{10}$$

While the cementation factor m describes the non-uniformity of the section of the conductive channels, the electrical tortuosity τ relates to the complexity of the path followed by the electrical current (e.g. Guéguen and Palciauskas, 1992) or, in a more general sense, the efficiency of electrical flow processes (Clennell, 1997). In hard, low-porosity rocks, the average electrical tortuosity is generally of the order of 10 (Pezard et al., 1991, 1999). For the ODP Leg 118 gabbro samples, Pezard et al. (1991) proposed a relationship similar to that of the less-altered mid-ocean ridge basalts from ODP Hole 504b (Pezard, 1990):

$$F = 8.04\phi^{-1.08}. \tag{11}$$

4.3. Altered fraction

An estimate for the altered weight fraction (φ_w) of the matrix contributing to electrical conduction may also be derived from the analysis of surface electrical properties. The surface conductivity (C_s) and *CEC* are related (Eqs. (3) and (4); Waxman and Smits, 1968). In the case of clay–sand mixtures, Revil et al. (1998) propose to relate the effective or "mean" *CEC* of the porous media to that of the clays present in the formation via a mean clay weight-fraction (φ_w):

$$CEC = \varphi_w \sum \chi_i CEC_i, \tag{12}$$

where CEC_i are the respective values of *CEC* for the various types of clay, and χ_i the corresponding clay volume fractions.

In this study, the notion of alteration is related to the surface electrical properties of alteration phases in gabbros, such as smectites, illites or zeolites (Shipboard Scientific party, 1999b) but also to the small size of secondary particles with respect to that of primary phases such as plagioclase or clinopyroxene. The notion of clay fraction (φ_w) is here extended to that of altered fraction for igneous rocks from ODP Hole 735B, keeping in the model only one alteration phase. Eq. (12) consequently becomes:

$$CEC = \varphi_w CEC_{alt} \tag{13}$$

where CEC_{alt} is that measured from cobalthexamine titration on the fraction <150 μm for each sample. As the effective *CEC* is related to the effective surface conductivity (C_s) by Eq. (6), the altered fraction (φ_w) is obtained directly from Eq. (13) and:

$$C_s = \tfrac{2}{3}\varphi_w \beta_s \rho_m CEC_{alt} \tag{14}$$

with β_s as defined above for an electrolyte with sodium cations only, while C_s, ρ_m and CEC_{alt} are measured independently in the laboratory on the same sample. The altered fraction φ_w is then computed for each sample. In summary, this new method leads to a quantitative evaluation of the

altered weight fraction of a crystalline rock based on electrical properties measurements.

5. Core measurements

5.1. Density and porosity

Porosity, bulk density, and grain density (Table 2) were obtained from triple weighing. For rocks with porosities lower than 1%, as most of the samples in this study, the absolute error is computed lower than 2% for densities (i.e. about ± 0.06 g/cm^3), and about 15% for porosity (i.e. $\leq \pm 0.1\%$ in porosity). The relative error is, however, much smaller, due to the uniformity of the sample set.

5.2. Electrical measurements

In order to distinguish between the electrolytic and the surface conduction mechanisms, the sample set was analysed with measurements of electrical resistivity performed at variable saturating fluid salinity (seven series of measurements, from 0.05–100 g/l). The intrinsic electrical formation factor F of each sample, as well as surface conductivity parameters (Table 2; Waxman and Smits, 1968; Pezard, 1990; Revil and Glover, 1998) have been extracted on the basis of the RG model (Revil and Glover, 1998), giving for the derivation the same weight to each of the measurements (Fig. 2). While the electrical measurements for ODP Leg 118 samples were done at 50 Hz (Pezard et al., 1991), those for Leg 176 samples were done at 100 Hz. This frequency value was chosen to be similar to that used for downhole measurements with the Dual Laterolog (Pezard, 1990; Pezard et al., 1991).

The electrical properties for ODP Leg 118 samples were initially analysed on the basis of the WS model (Waxman and Smits, 1968) and limited to the determination of the formation factor F. An estimate for surface conduction was obtained using Eq. (4), with constant B and μ values. As μ could not be determined in the laboratory, Pezard et al. (1991) erroneously concluded that $\mu = 10$ was an acceptable value for surface tortuosity. This assumption produced a negligible contribution of surface conductivity (about 0.5% for fresh samples) with respect to the electrolytic component, which is proven to be wrong subsequently in this paper. This effect was amplified by the lack of low salinity measurements in the ODP Leg 118 data set (Fig. 2c). The more precise RG model used here leads to a combined

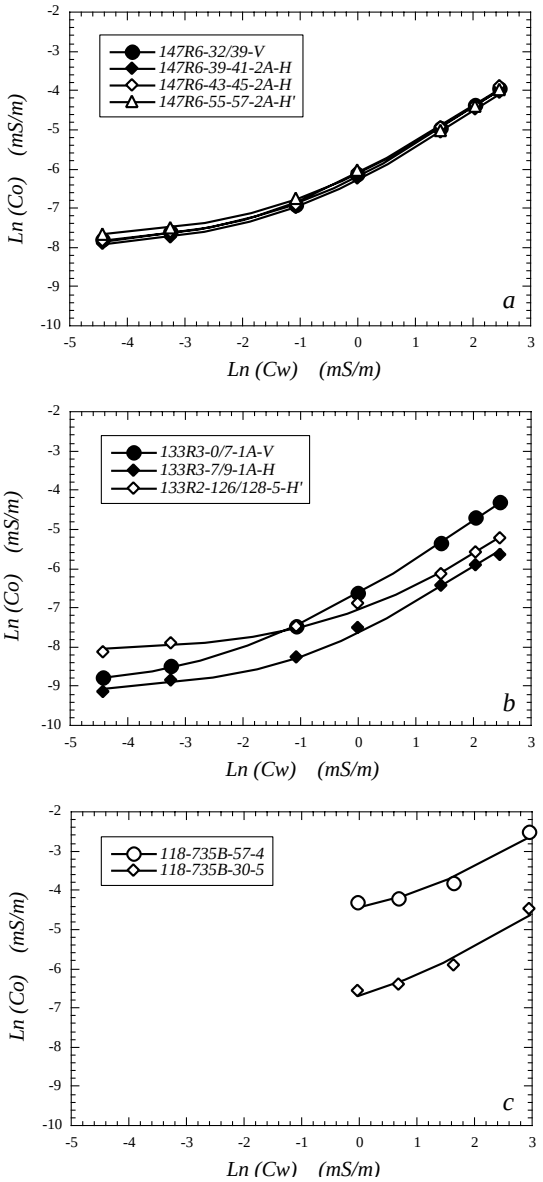

Fig. 2. Examples of plots of the core conductivities as a function of the saturating fluid conductivities. Best fit curves are calculated using Revil and Glover model (1998). (a) Leg 176 samples from core147 section 6; very weak anisotropy. (b) Leg 176 samples from core 133 section 3; strong anisotropy. (c) Leg 118 samples from cores 30 and 57, sections 4 and 5, respectively.

Table 2
Laboratory measurements and derived parameters

Sample ID	Depth (mbsf)	Grain density (g/cm^3)	Porosity ϕ (%)	F (RG 98)	C_s (RG 98) (mS/m)	Tortuosity τ ($F\phi$)	Cementation index m	CEC (cmol/kg)	φ_w (%)	Mag. Susc. K (10^{-3} SI)	Mag. susc. K (shipboard) (10^{-3} SI)	V_p (m s^{-1})
118-735B-06-1	20	2.91	1.1	1471	1.34	16.2	1.62	4.8	2.96	–	–	–
118-735B-12-1	40	2.83	2.9	520	4.22	15.1	1.77	1.2	38.33	–	–	–
118-735B-14-2	52.47	3	1.7	1233	2.22	21	1.75	1.2	19.02	–	–	–
118-735B-22-4	98.87	2.95	2.8	580	5.07	16.2	1.78	1.1	48.19	–	–	–
118-735B-30-5	142.98	2.99	0.7	2225	0.57	15.6	1.55	5.8	1.01	–	–	–
118-735B-31-3	146.43	3	1	1567	0.42	15.7	1.6	4	1.08	–	–	–
118-735B-32-4	152.31	2.79	1.4	1155	2.45	16.2	1.65	4.2	6.45	–		–
118-735B-40-1	191.45	2.93	1.1	1245	1.51	13.7	1.58	2.6	6.11	–	–	–
118-735B-41-4	201.36	2.99	0.7	1941	0.8	13.6	1.53	1.2	6.88	–	–	–
118-735B-47-3	225	3.01	0.8	1686	0.7	13.5	1.54	2.8	2.56	–	–	–
118-735B-48-1	231.93	3.24	1.1	641	–	7.1	1.43	2.3	–	–	–	–
118-735B-50-4	242.81	3.17	0.5	870	–	4.3	1.28	1.9	–	–	–	–
118-735B-53-2	254.86	3.2	0.8	929	–	7.4	1.42	2.6	–	–	–	–
118-735B-53-4	257.83	2.95	1.8	827	3.61	14.9	1.67	3.7	10.2	–	–	–
118-735B-56-2	272.37	3.26	0.9	431	–	3.9	1.29	2.2	–	–	–	–
118-735B-57-4	279.59	2.87	4.5	325	6.6	14.6	1.87	5.4	13.14	–	–	–
118-735B-58-2	281.96	3	0.9	1518	0.45	13.7	1.56	2.3	2.01	–	–	–
118-735B-61-4	300.77	2.9	1.4	846	0.63	11.8	1.58	2.5	2.68	–	–	–
118-735B-63-1	306.43	2.89	2.9	575	3.64	16.7	1.79	2.8	13.87	–	–	–
118-735B-72-5	363.86	3	0.7	2085	0.61	14.6	1.54	1.4	4.48	–	–	–
118-735B-73-5	371.41	2.99	0.9	1619	0.53	14.6	1.57	1.5	3.65	–	–	–
118-735B-77-3	407.83	2.95	0.8	2223	0.53	17.8	1.6	2.2	2.52	–	–	–
118-735B-78-2	411.68	2.91	3.1	504	5.11	15.6	1.79	2.6	20.83	–	–	–
118-735B-79-5	420.48	3.18	0.8	269	–	2.2	1.16	3	–	–	–	–
118-735B-80-7	432.85	3.26	0.7	855	–	6	1.36	2.6	–	–	–	–
118-735B-85-5	477.76	2.94	3.3	493	4.93	16.3	1.82	3	17.24	–	–	–
118-735B-86-5	488.25	2.88	0.9	1386	0.72	12.5	1.54	1.4	5.51	–	–	–
118-735B-86-6	488.43	2.81	1.1	1175	0.67	12.9	1.57	3.7	1.99	–	–	–
118-735B-87-1	491.38	3.28	1.2	636	–	7.6	1.46	2.8	–	–	–	–
176-735B-96-2-49/51 (H′)	550.29	2.96	0.87	1707	0.49	14.9	1.57	–	–	16.55	14.76	7028
176-735B-96-2-54/58 (V)	550.34	3.08	0.92	2477	–	22.8	1.67	5.6	–	70.76	–	6602
176-735B-116-4-127/129 (H)	677.04	2.97	0.59	2451	0.08	14.5	1.52	2	0.39	5.34	–	7020
176-735B-116-4-129/133 (V)	677.06	2.97	0.5	2543	0.07	12.7	1.48	2.5	0.29	4.55	–	7137
176-735B-116-5-7/9 (H′)	677.27	2.93	0.75	2312	0.07	17.3	1.58	–	–	2.56	2.51	7182
176-735B-133-2-126/128 (H′)	825.5	2.95	0.73	2388	0.3	17.4	1.58	–	–	6.39	5.99	7015
176-735B-133-3-0/7 (V)	825.63	2.99	1.49	902	0.12	13.4	1.62	2	0.62	6.19	–	7086
176-735B-133-3-7/9 (H)	825.7	2.95	0.44	3148	0.1	13.9	1.48	2	0.52	5.38	–	7163
176-735B-142-3-86/88 (H′)	896.47	3.03	1.04	786	0.45	8.2	1.46	–	–	13	3.29	6995
176-735B-142-5-0/6 (V)	898.44	2.93	0.87	839	0.31	7.3	1.42	–	–	5.77	–	6614
176-735B-142-5-6/8 (H)	898.5	2.94	0.76	1169	0.36	8.9	1.45	–	–	5.12	–	6411
176-735B-147-6-32/39 (V)	947.26	2.96	0.74	664	0.34	4.9	1.32	1.8	1.97	5.98	–	6208
176-735B-147-6-39/41 (H)	947.33	2.94	0.81	730	0.31	5.9	1.37	1.7	1.94	3.35	–	6378
176-735B-147-6-43/45 (H′)	947.37	2.94	0.82	627	0.33	5.1	1.34	1.6	2.18	3.57	–	6441

Table 2 (*continued*)

Sample ID	Depth (mbsf)	Grain density (g/cm^3)	Porosity ϕ (%)	F (RG 98)	C_s (RG 98) (mS/m)	Tortuosity τ ($F\phi$)	Cementation index m	CEC (cmol/kg)	φ_w (%)	Mag. Susc. K (10^{-3} SI)	Mag. susc. K (shipboard) (10^{-3} SI)	V_p (m s^{-1})
176-735B-147-6-55/57 (H′)	947.49	2.95	1.09	666	0.41	7.3	1.44	–	–	7.59	6.97	6462
176-735B-154-5-32/34 (H′)	1010.59	2.95	0.96	875	0.34	8.4	1.46	–	–	6.38	6.29	6605
176-735B-154-5-42/44 (H)	1010.69	2.97	0.66	1063	0.38	7	1.39	–	–	11.14	–	6419
176-735B-154-5-44/50 (V)	1010.71	2.94	0.81	890	0.41	7.2	1.41	2.2	1.96	8.69	–	6530
176-735B-158-4-65/67 (H′)	1048.63	2.97	0.4	781	0.37	3.1	1.21	–	–	6.83	7.19	6195
176-735B-158-4-80/84 (V)	1048.78	2.98	0.83	656	0.39	5.4	1.35	–	–	4.71	–	6520
176-735B-158-4-84/86 (H)	1048.82	3.01	0.9	602	0.48	5.4	1.36	–	–	4.19	–	6698
176-735B-166-1-21/23 (H′)	1111.11	2.96	1.13	829	0.36	9.4	1.5	–	–	3.37	3.34	6690
176-735B-167-6-103/107 (V)	1128.28	2.94	0.67	1151	0.31	7.7	1.41	–	–	2.11	–	6993
176-735B-167-6-109/112 (H)	1128.34	2.97	0.58	1053	0.31	6.1	1.35	2	1.63	2.34	–	6774
176-735B-168-2-10/12 (H′)	1131.49	2.98	0.85	691	0.6	5.9	1.37	–	–	7.21	2.47	6683
176-735B-179-5-90/97 (V)	1227.35	2.92	0.59	966	0.71	5.7	1.34	2	3.75	9.33	–	6716
176-735B-179-5-97/99 (H)	1227.42	2.9	0.64	948	0.52	6.1	1.36	1.3	4.22	7.25	–	6688
176-735B-179-5-110/112 (H′)	1227.55	2.96	0.72	1413	0.24	10.2	1.47	–	–	4.26	4.32	6941
176-735B-190-4-67/69 (H′)	1330.9	2.99	0.73	1109	0.27	8.1	1.43	–	–	2.19	2.15	6863
176-735B-190-4-80/86 (V)	1331.03	2.95	0.67	1059	0.28	7.1	1.39	1.7	1.71	6.29	–	6622
176-735B-190-4-87/89 (H)	1331.1	2.97	1.25	617	0.52	7.7	1.47	2	2.7	1.92	–	6642
176-735B-209-7-97/99 (H′)	1497.16	3.01	0.89	979	0.43	8.7	1.46	–	–	2.69	–	6733
176-735B-209-7-100/102 (H)	1497.19	3	0.73	901	0.61	6.6	1.38	2.2	2.83	1.79	–	6581
176-735B-209-7-102/108 (V)	1497.21	3	0.89	886	0.92	7.9	1.44	2	4.74	3.15	–	6690
Mean (Leg 118)		3	1.47	1098	2.15	12.8	1.57	2.7	10.49	–	–	–
Standard deviation (Leg 118)		0.14	1.01	583	1.97	4.6	0.17	1.2	12.27	–	–	–
Median (Leg 118)		2.99	1.1	929	1.07	14.6	1.57	2.6	5.81	–	–	–
Mean (Leg 176)		2.97	0.8	1202	0.37	9.1	1.44	2.2	2.1	7.59	5.39	6715
Standard deviation (Leg 176)		0.03	0.22	684	0.18	4.3	0.09	1	1.37	11.63	3.63	267
Median (Leg 176)		2.96	0.79	925	0.36	7.7	1.44	2	1.96	5.36	4.32	6689
Mean (all)		2.98	1.11	1154	1.08	10.8	1.5	2.5	7.09	7.59	5.39	6715
Standard deviation (all)		0.1	0.77	637	1.52	4.8	0.15	1.2	10.3	11.63	3.63	267
Median (all)		2.96	0.87	929	0.48	9.4	1.47	2.2	2.83	5.36	4.32	6689

determination of the electrical formation factor F and surface conductivity C_s for each sample.

In the present analysis, the uncertainty on C_s is higher for ODP Leg 118 samples than for those from Leg 176 due to the lack of measurements made at low salinity of the saturating fluid in the former case (Fig. 2c). The measurements on all samples were done with 2 electrodes. This experimental set-up is more sensitive to the polarising effect at the electrode/sample interface than a 4 electrode device. Nevertheless, this effect is reduced by using paper filter to separate the electrodes from the sample, and remains negligible at frequencies as low as 100 Hz (Pezard, 1990).

5.3. CEC measurements

Small pieces of the samples were crushed and sifted to extract the finest fraction (<150 μm), which is here approximated to represent the altered fraction of the rock. The *CEC* measurements were performed by the "Laboratoire d'Analyse des Sols" (LAS) of INRA at Arras (France), by cobalthexamine titration of the extracted fraction (Table 2). The precision is of the order of 0.1 meq/100 g (0.1 cmol/kg).

5.4. Acoustic velocity measurements

Compressional velocity (V_p) measurements were performed for each of the Leg 176 samples at 2.25 MHz, using a Panametrics Epoch III-2300 device. The Teflon jackets used for the electrical measurements were kept in place, in order to reduce the influence of desaturation during the measurements. The samples were measured while saturated with a 30 g/l NaCl solution. The precision of these measurements was determined as better than 1%, i.e. of the order of 50 m/s. The data are reported in Table 2.

5.5. Magnetic susceptibility

The Kappa-Bridge device of the magnetic laboratory at CEREGE was used under scalar mode for measuring the bulk magnetic susceptibility (Table 2). This measurement proves to be particularly useful to detect the presence of metallic oxides (Shipboard Scientific party, 1999a), as in the case of only one of the 34 samples collected during ODP Leg 176.

6. Results

All data from mini-core measurements and derived calculated parameters (see above) are displayed in Tables 2 and 3.

6.1. Grain density, magnetic susceptibility and formation factor

Grain density is very homogeneous, with an average of 2.96 g/cm^3 in fresh samples; it increases to 3.23 g/cm^3 on average in ODP Leg 118 Ox-rich

Table 3
Anisotropy of F, C_s, and V_p in the core reference frame ((V−H)100/mean(V,H); negative when higher horizontally.

Sample ID	Depth (mbsf)	Anisotropy of F (V & H, %)	Anisotropy of C_s (V & H, %)	Anisotropy of V_p (V & H, %)
176-735B-96-2-54/58	550.34	–	–	–
176-735B-116-4-127/133	677.05	3.7	−6.2	1.7
176-735B-133-3-0/9	825.66	−110.9	17.4	−1.1
176-735B-142-5-0/8	898.47	−32.9	−16.9	3.1
176-735B-147-6-32/41	947.3	−9.5	9.2	−2.7
176-735B-154-5-42/50	1010.7	−17.7	8.4	1.7
176-735B-158-4-80/86	1048.8	8.6	−19.6	−2.7
176-735B-167-6-103/112	1128.3	8.9	−2	3.2
176-735B-179-5-90/99	1227.4	1.9	31.5	0.4
176-735B-190-4-80/89	1331.07	52.7	−60.7	−0.3
176-735B-209-7-100/108	1497.2	−1.7	41.4	1.6
Mean (Leg 176)		−9.7	0.3	0.5
Standard deviation (Leg 176)		41.9	29	2.2
Median (Leg 176)		0.1	3.2	1

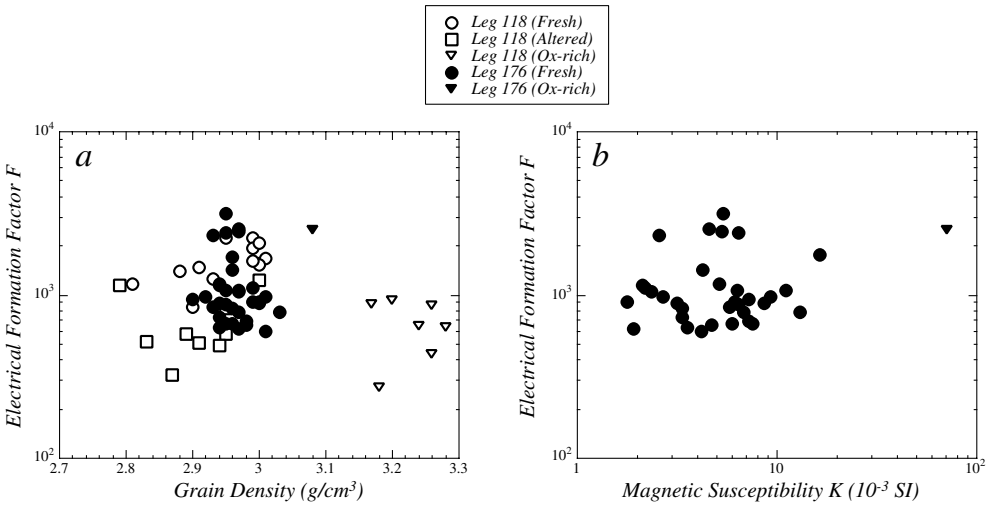

Fig. 3. Electrical formation factor as a function of: (a) grain density; and (b) magnetic susceptibility.

samples, and decreases to 2.90 g/cm^3 on average in Leg 178 altered samples (Fig. 3a). As defined above, the electrical formation factor F characterises the ratio between the bulk electrical conductivity and the electrical conductivity of the saturating fluid; the saturated rock gets more conductive as F decreases. Fig. 3a shows that, globally, the presence of altered phases or oxides does seem to affect F significantly, although a few points for altered and Ox-rich samples have lower F than fresh samples. This is confirmed by the absence of correlation between F and the bulk magnetic susceptibility K (Fig. 3b). As expected, K depends primarily on the presence of oxides.

6.2. Acoustic compressional velocity

The acoustic velocity measurements are compared, in Fig. 4, to previous measurements in ODP Leg 118 samples (Iturrino et al., 1991). Our room pressure V_p data, obtained on saturated samples, are consistent with previous data at low confining pressure (40 MPa), obtained on both dry and saturated samples. At higher confining pressure (100 MPa), beyond the closure of most cracks in the samples, V_p values were slightly higher (Fig. 4c), but remain similar to our data (Fig. 4b).

6.3. Porosity structure, surface conductivity and alteration

Porosity is low in most samples (Fig. 5a), especially in those collected during Leg 176, where it is 0.8% on average. Higher porosities correspond to the "tectonised" samples of ODP Leg 118 (2.71% on average) and are related to higher alteration. Except for the Ox-rich samples, all ODP Leg 118 samples, together with part of the Leg 176 samples, show a classical correlation between F and ϕ (e.g. Pezard et al., 1991), F increasing with decreasing ϕ, the product of these two properties being defined as the electrical tortuosity τ (see above). The best fit for this group of well correlated samples is given by $\tau = 15$. The relationship between F and ϕ proposed by Pezard et al. (1991) is given for comparison, as well as Archie's law, which is not valid for gabbroic rocks (Fig. 5a). The Leg 176 samples aligning with ODP Leg 118 ones in Fig. 5a are those from the upper part of the Leg 176 section. A second group, comprising the samples from the lower part of Leg 176 and the Ox-rich samples from ODP Leg 118, clusters around an average value of $\tau = 10$, with no obvious correlation between τ and ϕ (Fig. 5a). This may be partly due to the fact that the Leg 176 samples are fresh, with little variations in both V_p and ϕ (see also Table 2). While porosity appears to have a significant influence on the

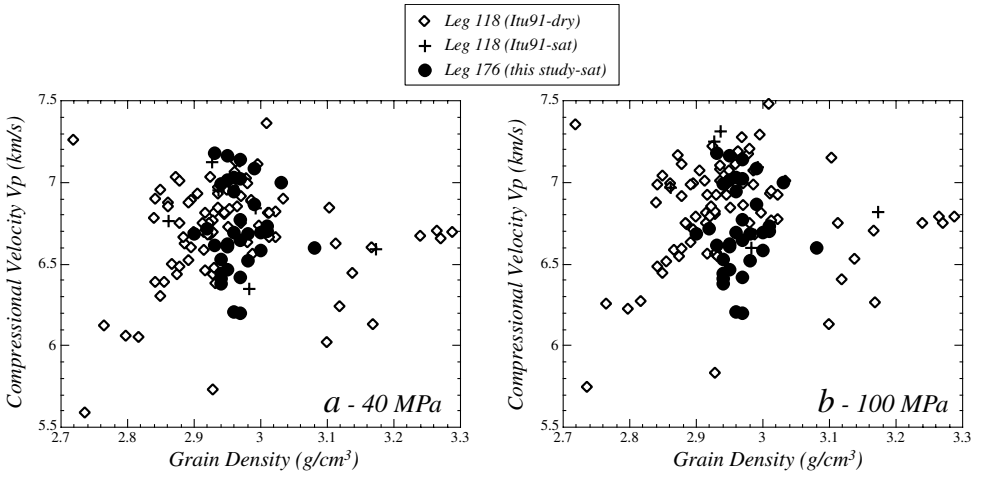

c	Leg 176 - sat	itu91 - sat		itu91 - dry	
		40 MPa	100 MPa	40 MPa	100 MPa
mean Vp	6.71	6.77	7.01	6.69	6.82
standard deviation	0.27	0.27	0.27	0.31	0.31
median Vp	6.69	6.80	7.03	6.75	6.85

Fig. 4. Acoustic compressional velocity as a function of grain density. The Leg 176 data (this study), on saturated samples at room pressure and room temperature are shown together with previous data from Leg 118 (Iturrino et al., 1991), on dry and saturated samples, under confining pressures of: (a) 40 MPa; and (b) 100 MPa. Mean, standard deviation, and median values for the three groups of data are given in (c).

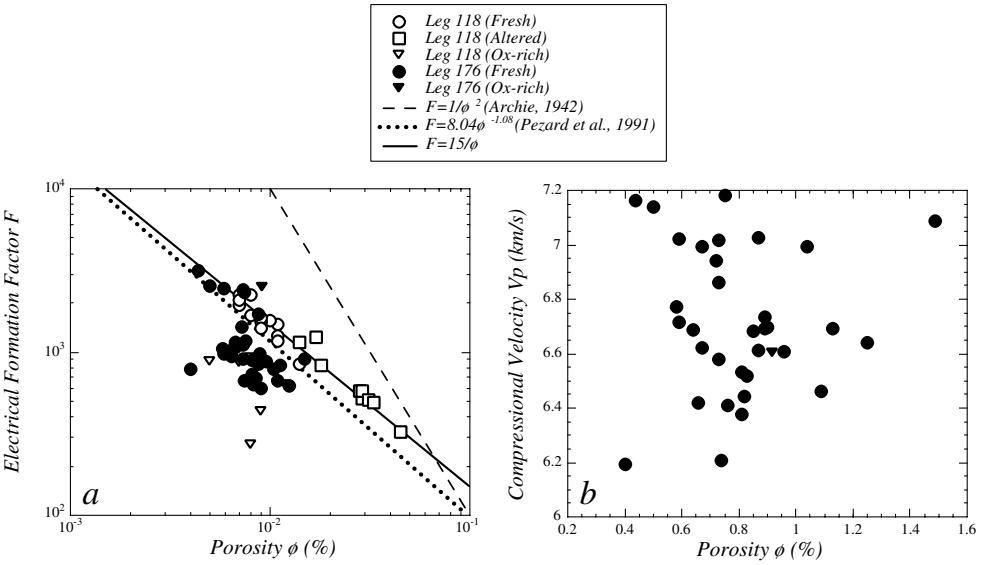

Fig. 5. Influence of porosity on: (a) the electrical formation factor; and (b) the acoustic compressional velocity. F and ϕ are strongly correlated, with $F\phi$ defining the electrical tortuosity, while there is no correlation between V_p and ϕ. The Leg 176 points aligned with the Leg 118 ones in (a) are those of the upper part of the Leg 176 section of 735B (samples from cores 96, 116, and 133).

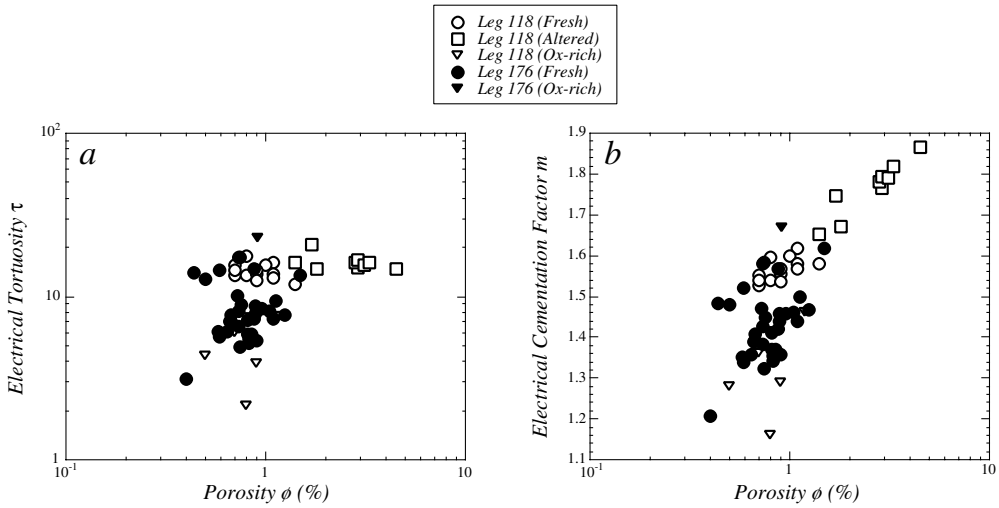

Fig. 6. Correlations: (a) between the electrical tortuosity and the porosity; and (b) between the electrical cementation factor and the porosity. The Leg 176 points aligned with the Leg 118 ones correspond to the upper part of the Leg 176 section of 735B (samples from cores 96, 116, and 133).

transport properties, there is no clear correlation between V_p and ϕ (Fig. 5b).

The two parameters characterising the porosity structure (τ and m), when plotted against ϕ (Fig. 6), display the same partitioning as Fig. 5a, with the same group of samples linearly correlated, and a second one clustering around lower values of τ and m. The porosity structure of the Ox-rich samples (except for one sample, from core 96 section 2), which have lower τ and m than the surrounding rocks, is probably modified and simplified by the crystallisation of oxides. On the one hand, τ is nearly constant ($\sim$15) in the upper part of ODP hole 735B; it is lower and more variable in its lower part (Fig. 6a). On the other hand, m varies exponentially with ϕ in the upper part of the hole (Fig. 6b). The second group (lower part of Leg 176) may also display a correlation between m and ϕ, with a steeper slope, although it is much less clear than for the upper part of the hole, due to the homogeneity of ϕ in Leg 176 samples. Fig. 7 shows the relationships between the porosity structure (τ and m) and the alteration, as revealed by the electrical surface conductivity (Fig. 7a and b) and the derived altered fraction (Fig. 7c and d). Again, there is a clear partition between the upper and the lower part of the hole when looking at τ as function of C_s (Fig. 7a) or φ_w (Fig. 7c), with C_s and φ_w nearly constant in the lower part, while they vary of more than two order of magnitude in the upper part. Similarly, m increases, as a function of C_s and φ_w, essentially in the upper part of the hole, as shown by the most altered samples (Fig. 7b and c). In addition to the differences between the upper and the lower parts of ODP hole 735B, which are further discussed later, Figs. 6 and 7 together indicate that, in the upeer part of the hole, the porosity structure, and consequently the electrical pathways are mostly related to a primary microstructural network, such as grain boundaries, since the change in porosity and alteration do not affect the tortuosity. The evolution of the porosity structure with time, hydrothermal circulation and alteration is restricted to a volume change (increase in ϕ) and an increase in m, indicating a higher variability of the channel thicknesses in the porous network, including restrictions.

We estimate the percentage contribution to the total effective conduction by surface conduction by using the parameter $\beta = (FC_s)/(FC_s) + C_w$ and assigning a value of 5000 mS/m for C_w (for sea water at 24°C). Fig. 8a shows a partition of the samples in three groups. The most altered samples from ODP Leg 118, as expected, have the higher β, with an average value of 33.6%. β decreases to 18.2% on average in the fresh samples of ODP Leg 118, and to 6.7% in Leg 176 samples. This may be explained by the

combination of the higher homogeneity of the Leg 176 sampling and a possible decrease of bulk alteration downhole, as discussed below. For the most altered samples, β does not depend on F; it becomes correlated to F for most of the freshest rocks (Fig. 8b). Since the topology of the porous network does not vary much (τ in Figs. 6 and 7) this positive correlation must be related to local decreasing thickness of the conduits when alteration increases.

6.4. Anisotropy of F, C_s and V_p

The 2D anisotropy in the core reference frame (see description of the cores) has been calculated for F, C_s, and V_p, and is reported in Table 3. Fig. 2a and b illustrate the large difference in electrical anisotropy for the Leg 176 samples. However, we do not find any good correlation of the magnitude of anisotropies with the shipboard observations such as the intensity of magmatic or plastic foliations, the background alteration (Table 1), or the grain size. The best possible correlation relates the anisotropy of F to the intensity of plastic foliation *Pf* estimated macroscopically onboard ship (Fig. 9a). This is consistent with the conclusion given above that the electrolytic conduction occurs in a porous network mostly controlled by primary microstructures such as the grain boundaries, and thus by the mineral foliations. The scattering of

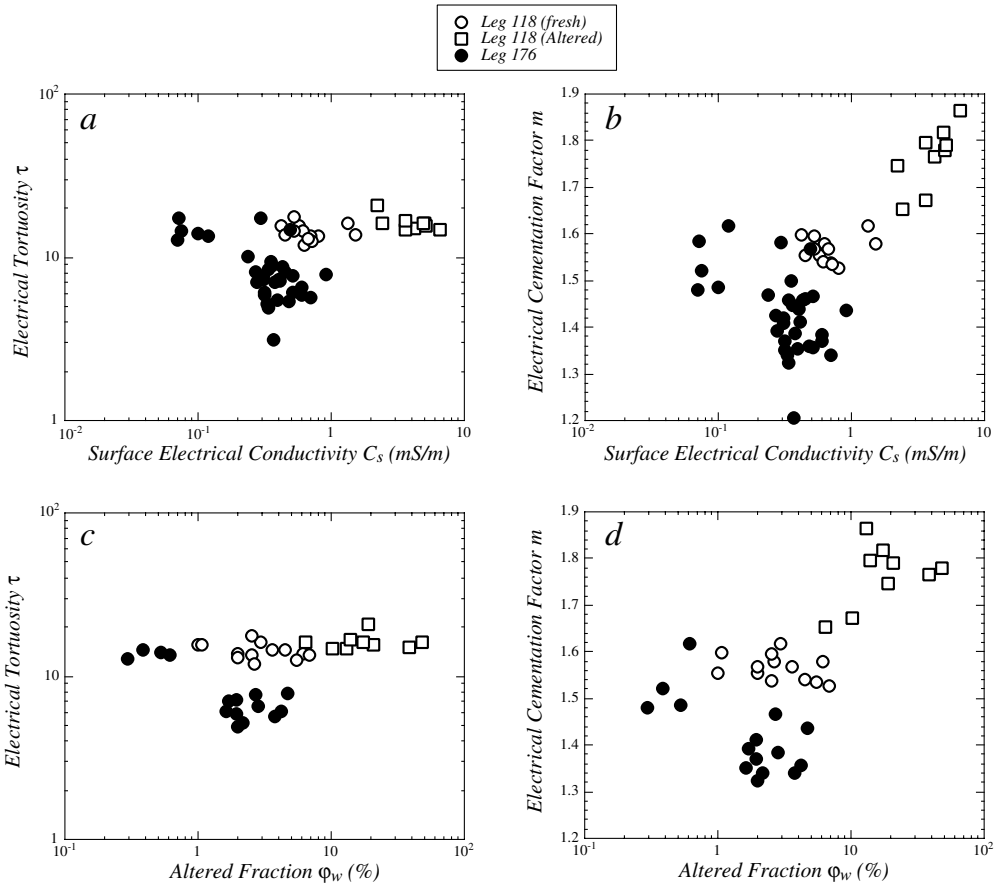

Fig. 7. Correlations: (a) between the electrical tortuosity and the surface electrical conductivity; (b) between the electrical cementation factor and the surface electrical conductivity; (c) between the electrical tortuosity and the altered fraction derived from C_s and *CEC*; and (d) between the electrical cementation factor and the altered fraction derived from C_s and *CEC*. The Leg 176 points aligned with the Leg 118 ones in (a) and (c), and in the upper left half-side of (b) and (d) are those of the upper part of the Leg 176 section of 735B (samples from cores 96, 116, and 133).

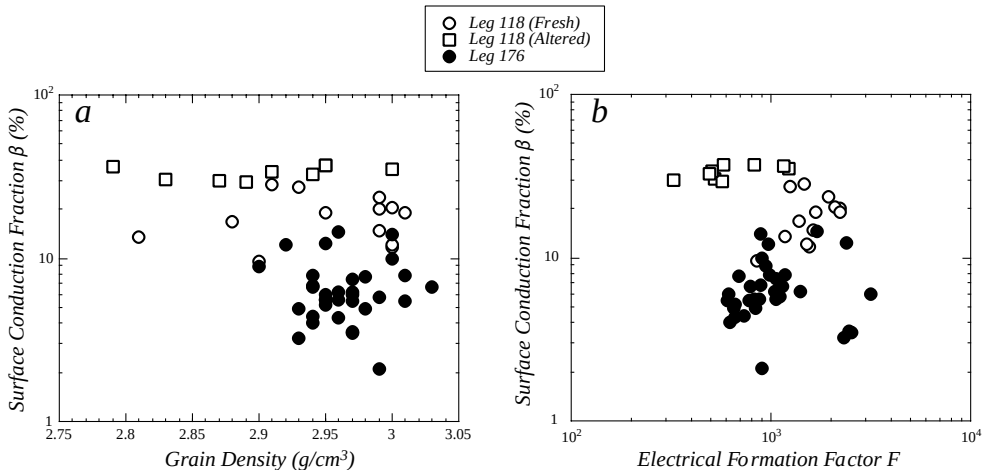

Fig. 8. Surface conduction fraction as a function of: (a) grain density; and (b) electrical formation factor.

points, with a change in F of about one order of magnitude for a given value of *Pf* may be explained by the fact that the *Pf* dip is always oblique to the core reference frame (Table 1). The anisotropy of V_p is not correlated to *Pf* (Fig. 9b). Seismic anisotropy of gabbros, when only controlled by the crystallographic preferred orientation, is expected to be weak, due to the opposite effects of plagioclase on the one hand, and pyroxene and olivine on the other hand (Mainprice, 1997; Lamoureux et al., 1999). Therefore, even small changes in the respective amounts of plagioclase and pyroxene + olivine may cause a switch of the anisotropy with respect to the foliation. This uncertainty on the sense of the anisotropy is reinforced here by the obliquity of *Pf* in the core reference frame. Moreover, the anisotropy of V_p must also be partly controlled by the cracks present in the minicores. Finally, the inverse correlation between the magnitude of V_p anisotropy and the magnitude of C_s anisotropy (Fig. 9c) reveals that these two anisotropies are primarily related to different microstructures; the influence of the crystallographic preferred orientation on the anisotropy cannot be neglected. This needs to be investigated through fabric measurements and modelling of the seismic properties of the measured samples. This study is under progress and will be the topic of another paper (Ildefonse et al., in prep.). Another problem with our characterisation of anisotropy, is that one cannot exclude a slight difference in microstructure, such as the crack density and/or orientation, that will affect significantly the measured properties. This discussion on the anisotropy will benefit from a comparison with acoustic measurement data under confining pressure (Iturrino et al., 2000), and would also benefit from further measurement of anisotropy on single cores.

7. Discussion. Downhole variations of physical properties

One of the main results of our investigations of electrical properties of ODP hole 735B samples is the partitioning of the porosity structure in two groups (Figs. 5–7). This partitioning is a function of depth. This must have relationships with the overall structure and/or alteration of the 735B crustal section. Fig. 10 shows the variations of the investigated properties with depth. The first point to emphasise is that there is apparently no discrepancy between the ODP Leg 118 (Pezard et al., 1991) and the ODP Leg 176 samples that could be related to the differences in the experimental method and conditions (see earlier and Fig. 2), since at least one sample group (from core 96 section 2) on top of the leg 176 section always plots in continuity with the ODP Leg 118 data (Fig. 10). While the grain density and porosity do not vary significantly downhole (Fig. 10a and b), the electrical tortuosity and cementation factor both show a sharp change toward lower values (i.e. simpler porous

network and more efficient electrical transport) for fresh samples around 850 mbsf (Fig. 10e and f). This change in porosity structure also reflects in the formation factor log (Fig. 10c), although one sample at 825 mbsf (core 133 section 3) already shows lower F value. A sharp change is also seen in the surface electrical conductivity, but at smaller depth (around 600 mbsf). However, unlike F, τ and m, C_s rapidly returns to values similar to the ones of fresh samples of ODP Leg 118 (Fig. 10d). The same trend is seen in the altered fraction log (Fig. 10g). The compressional velocity also show a sharp drop around 850 mbsf. V_p seems to be smaller on average below this depth. Finally, the magnetic susceptibility, as stated above, primarily reflects the oxide content of the rocks, and do not show a shift around 600–800 mbsf. From this series of logs, it clearly appears that the ODP hole 735B section is divided in two halves, nearly equal in thickness, with different porosity structures. This difference likely integrates the whole history of the gabbro section, from accretion to present-day alteration.

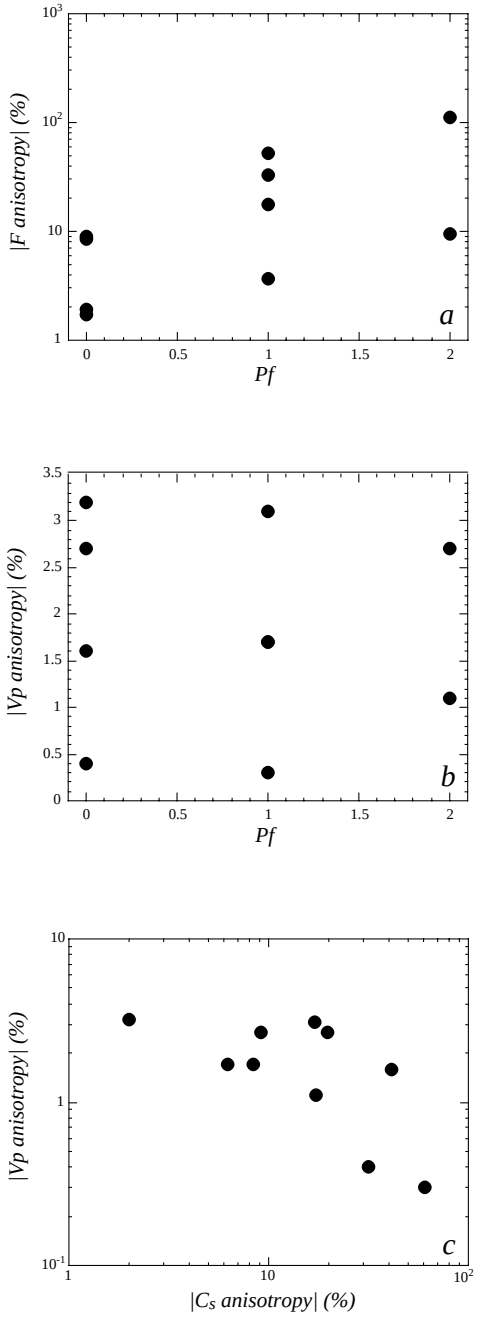

In Fig. 11, we tentatively correlate the downhole trends of the investigated properties with the main petrological and structural characteristics of ODP hole 735B gabbroic rocks, as summarised by Hirth et al. (2000). To F and V_p, we add here the contribution of surface conduction, characterised by β (see earlier), which also shows a shift toward lower values (see also Fig. 8) in the lower part of the hole, below 600 mbsf. The first striking similarity with the separation described above, is the overall lithological separation in two blocks, the lower one being mostly composed of less evolved troctolite, olivine gabbros and gabbros. Magmatic foliations are present along the whole section, with no significant changes. Plastic deformation is also present along the whole section, but it is mostly restricted to high-temperature shear zones in the lowermost half, below 700 mbsf approximately, while the upper part display retrograde (amphibolite facies) and semi-brittle shear zones (Fig. 11). Another striking feature is the occurrence, below 500 mbsf, of reverse shear zones, abundant between 900 and 1100 mbsf, which are never seen in the upper part. Therefore, during its tectono-magmatic history, part of the lower section undergoes

Fig. 9. (a) Magnitude of the anisotropy of F as a function of the intensity of plastic foliation Pf (shipboard observations); Pf intensity scale: 0 = no foliation, 1 = weakly foliated, 2 = strongly foliated (Shipboard Scientific party, 1999c). (b) Magnitude of the anisotropy of V_p as a function of P_f. (c) Magnitude of the anisotropy of V_p as a function of the magnitude of the anisotropy of C_s. Anisotropies (Table 3) are calculated in 2D, from measurements on mini-cores H and V only.

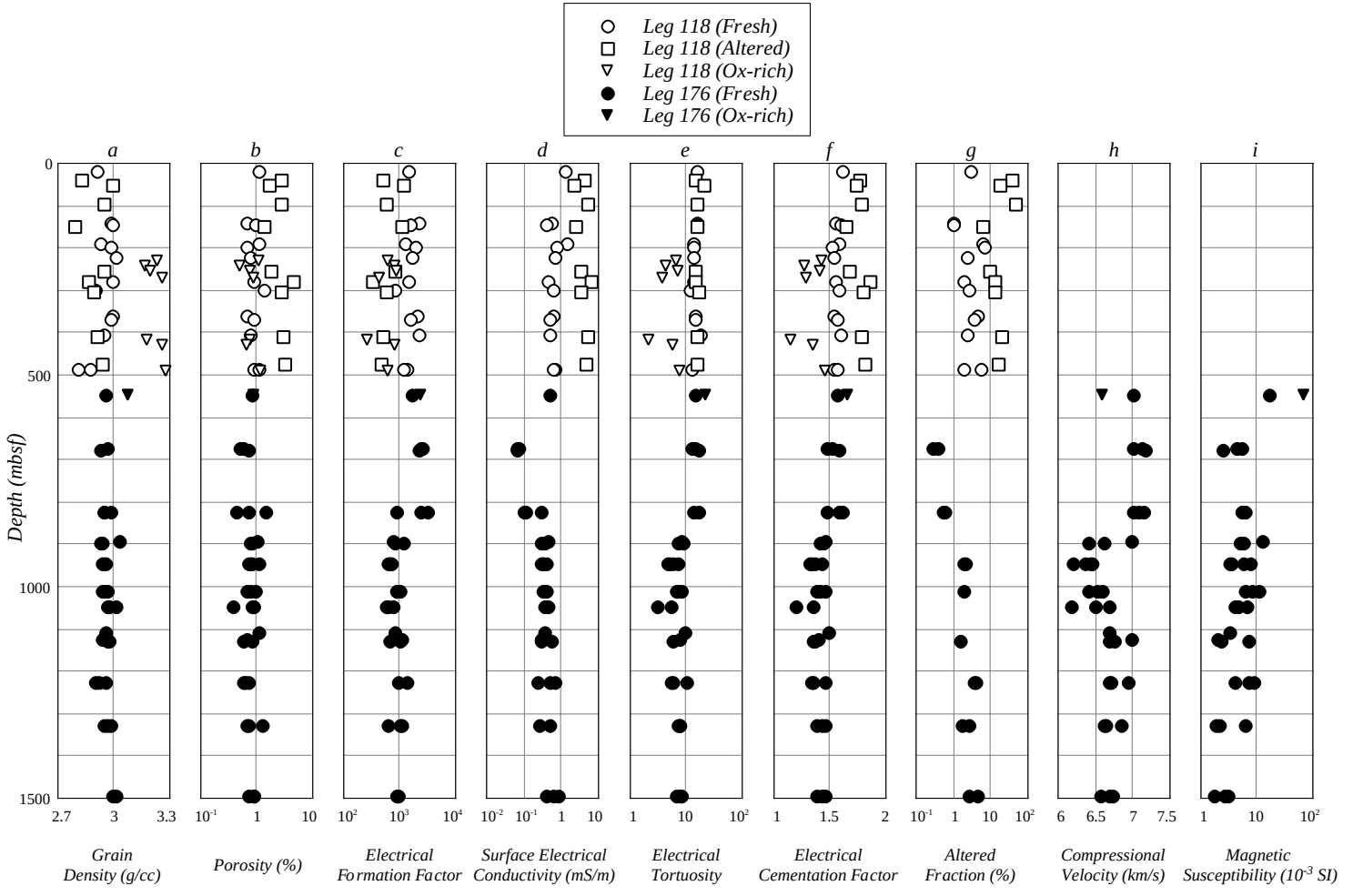

Fig. 10. Measured and calculated properties as a function of depth.

compression (see discussion in Hirth et al. 2000). The brittle deformation follows a similar logic, with reverse sense of slip in the lower half of the hole, mostly below 1000 mbsf. Thus, the observed difference in porosity structure could be related to distinct deformation history during accretion and unroofing of the 735B gabbros. Possible candidates for major discontinuities separating the two blocks are the two major brittle zones around 700 and 800 mbsf, the latter being a reflector in the VSP experiment performed during ODP Leg 118 (Swift et al., 1991). The transition depth is not very clear. From the trends of F, τ and m, it seems to occur around 850 mbsf, between samples of core 133 and 142; however, the shift in C_s and β occurs at shallower depth, below 600 mbsf (Fig. 10 and 11). Further sampling of this particular interval of the ODP hole 735B core is required to better define this transition depth.

Another way to explain the change in porosity structure would be to relate it to the difference in the stress regime suffered by the crust. From breakout studies in DSDP/ODP boreholes 395B and 504B, Moos and Zoback (1990) suggest that high horizontal stresses must exist at a relatively shallow depth ($<$1 km) into young oceanic crust, due to the low vertical charge. Consequently, the recent and present-day, low-temperature, hydrothermal alteration should occur mostly in the upper part ($<$1 km), along sub-horizontal channels. These could re-use pre-existing mechanical anisotropy related to the high-temperature (amphibolite facies) foliations in the upper 500 m of ODP hole 735B, especially abundant in the first 150 m, due to early low-angle detachment faulting (Shipboard Scientific party, 1999b; Hirth et al. 2000). Such an interpretation is apparently consistent with our data, since C_s and altered fractions are higher on average in the upper part of the hole (Fig. 10d and g, Fig. 11).

However, this interpretation is in contradiction with the shipboard observations of ODP Legs 118 and 176, which show that the polarity of metamorphic alteration in ODP hole 735B is reverse, compared to "normal" oceanic crust such as the one drilled at ODP hole 504B (Alt et al., 1993), with high-temperature assemblages most abundant at the top, and low-temperature assemblages dominant near the base of the recovered section. This contradiction maybe explained by: (i) a stress regime in the crust at ODP site 735 different from that described for sites 395 and 504 (Moos and Zoback, 1990), because of the proximity of the Atlantis transform zone for instance; and (ii) a lack of representative samples of the low-temperature alteration in the bottom part of the hole, since low-temperature fluid circulation is localised to a restricted set of fractures/cracks and associated local groundmass alteration (Shipboard Scientific party, 1999b). Therefore, we can also suggest that the data from the lower part of the hole, from about 850 mbsf, are related to the lower-temperature alteration described during Leg176, which would significantly affect the porosity structure, with very little variations in porosity and higher variations in the topology of the porous network than in the upper part of the hole, possibly due to cracks.

8. Conclusions and perspectives

The physical properties of a set of 63 gabbroic samples from ODP Hole 735B (SWIR), including 34 new samples from the lowermost 1000 m of the hole, have been measured in the laboratory, with a particular emphasis on the analysis of electrical properties.

The acoustic compressional velocities, measured in this study at room pressure on saturated samples, are in the same range than those previously measured on ODP Leg 118 samples (Iturrino et al., 1991). The anisotropy of V_p is weak, and does not correlate with plastic foliation intensities (Fig. 9b), probably because of the obliquity of the plastic foliations with respect to the core reference frame. The porosity is low in fresh samples ($<$1% on average), and increases to about 3% in altered samples from the upper part of the hole (ODP Leg 118 data set, Pezard et al., 1991).

Except for oxide-rich gabbros, the electrical formation factor of the samples from the upper part of the hole (down to at least 825 mbsf) is inversely correlated with the porosity, with a constant value of about 15 for the electrical tortuosity (Fig. 5a). The latter does not change much with deformation and/or alteration (Fig. 6 and 7), which indicates that the porosity structure is probably controlled by primary microstructures, such as grain boundaries. With time and alteration, the only changes are an increase in porosity and a higher variability of channel thicknesses,

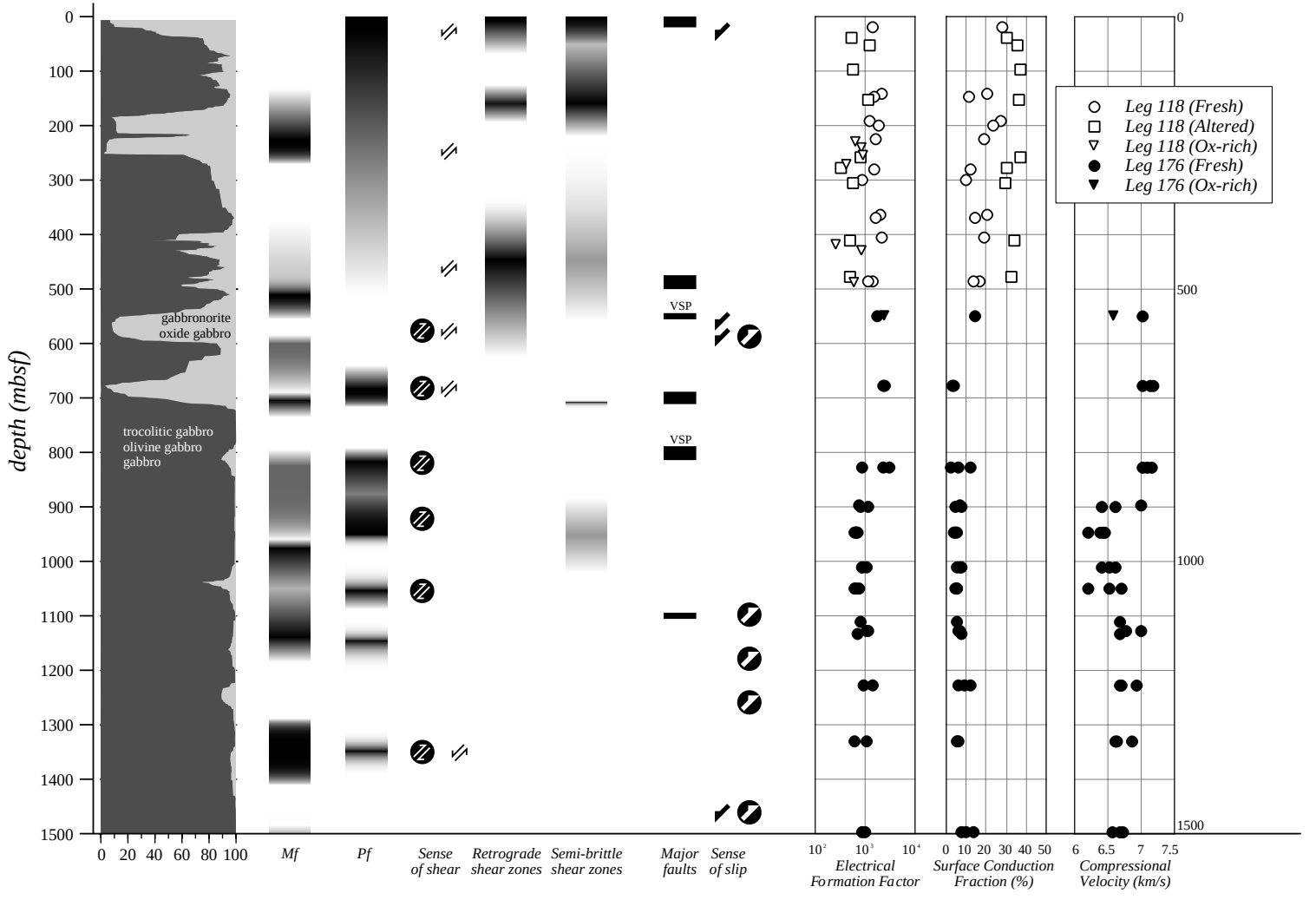

Fig. 11. Summary log, showing some petrological (after Shipboard Scientific party, 1999a) and structural characteristics of Hole 735B cores (after Hirth et al. 2000) as a function of depth, together with the electrical formation factor, the surface conduction fraction, and the acoustic compressional velocity. The grey intensity in *Mf*, *Pf*, retrograde and semi-brittle shear zone logs is proportional to the intensity of the fabrics. This figure illustrates the major change in petrological, structural, and microstructural (porosity structure) around 600–800 mbsf.

including reductions of the pore throat size, as indicated by the increase of the electrical cementation factor m (Fig. 6 and 7). The only change in the 3D topology of the porous network occurs in oxide-rich samples (with lower electrical tortuosity values), and is related to the crystallisation of the Fe–Ti oxides.

The electrical anisotropy is highly variable. A weak correlation is obtained between the anisotropy of F and the shipboard estimation of the plastic foliation intensity (Fig. 9a). This is consistent with previous conclusion that the porosity network is controlled by primary microstructures, which could then become more anisotropic as deformation proceeds.

In the lower part of the hole (below 850 mbsf), there is very little variation in porosity, while the 3D topology of the porous network changes, with a varying electrical tortuosity between 3 and 10, and lower values of the electrical cementation factor (Fig. 6 and 7), likely indicating a porosity network mostly controlled by cracks. This difference in porosity structure could be documented as well by microstructural investigations of the porous network in the studied samples, in impregnated thin sections for instance. Unfortunately, this was not possible so far as the samples were shared, and sent back to collaborators after measurements.

The change in topology of the porous network downhole may be explained several ways, and likely integrates the whole history of the crustal section cored at ODP site 735 since accretion, including plastic deformation related to unroofing of the lower crust gabbros along a low-angle detachment fault, cooling, and alteration due to hydrothermal flow at various temperatures. Our present data set does not allow to conclude on the cause of the segmentation in porosity structure. Furthermore, the depth of the transition between the two identified units is poorly constrained, since the sample density is the lowest in the critical interval, between 600 and 850 mbsf. A new sampling is thus required, that will include a set of altered samples from the lower part of the core, and a set of additional samples, closer to each other, in the interval 600–850 mbsf. These will be the object of a further study.

The additional sampling should also include a set of oxide-rich gabbros. As pointed out above, the conduction via electronic processes in metallic minerals is not taken into account in our analysis of the electrical properties. Therefore, our determination of C_s was not applied here to oxide-rich gabbro samples, with high values (46.5 mS/m on average, i.e. about 50 times higher than C_s in the other samples) that incorporate the oxide contribution of the bulk conductivity. No model allows one to include the effect of a conductive phase such as the Fe–Ti oxides in the studied gabbros, and a new constitutive law for electrical conduction is hence required here to account for the conductive phase in the mineral matrix. As in Pezard et al. (1991), we suggest

$$C_o = \frac{C_w}{F} + C_s + C_{ox}, \tag{15}$$

where C_{ox} is a constant related to the oxide content and connectivity for a given sample which does not depend on the salinity of the saturating fluid. Thus, the different contributions to the electrical conduction may still be identified, provided that the oxide contribution is independently estimated. To a first approximation, this may be achieved through the oxide content, which can itself be estimated through grain density or magnetic susceptibility measurements, as indicated by the excellent correlation between the shipboard continuous measurements of magnetic susceptibility and macroscopical estimations of oxide fractions (Shipboard Scientific party, 1999a). The identification of a valid proxy for gabbro alteration (C_s) should then lead to the computation of the determination of C_w/F, as C_o can be measured independently, either in the lab or in-situ with logging techniques.

Acknowledgements

We thank Daniel Hermite for his assistance and expertise during the (long) measurement sessions, Florence Einaudi for her help in the lab, and Christophe Nevado for the thin sections. This work was funded by CNRS-INSU (Groupe ad hoc OCEANS). We acknowledge reviews from P. Glover and M. Huenges who helped to improve the manuscript, and the technicians and crew of ODP Leg 176 for their assistance during the cruise. This is CNRS-INSU contribution no. 245.

References

Alt, J.C., Kinoshita, H., Stokking, L.B., et al., 1993. Proc. ODP, Init. Repts. 148., College Station, TX (Ocean Drilling Program).

Archie, G.E., 1942. The electrical resistivity log as an aid in determining some reservoir characteristics. J. Pet. Technol. 5, 1–8.

Becker, K., 1985. Large-scale electrical resistivity and bulk density of the oceanic crust, DSDP Hole 504B, Costa Rica Rift. In: Anderson, R.N., Honnorez, J., Becker, K. (Eds.), Init. Rep. DSDP. US Government Printing Office, Washington, pp. 419–427.

Brace, W.F., Orange, A.S., Madden, T.R., 1965. The effect of pressure on the electrical resistivity of water-saturated crystalline rocks. J. Geophys. Res. 70, 5669–5678.

Cannat, M., Mével, C., Stakes, D., 1991. Stretching of the deep crust at the slow-spreading Southwest Indian Ridge. Tectonophysics 190, 73–94.

Clennell, M.B., 1997. Tortuosity: a guide through the maze. In: Lovell, M.A., Harvey, P.K. (Eds.), Developments in Petrophysics. Geological Society Special Publication, London, pp. 299–344.

Dick, H.J.B., Meyer, P.S., Bloomer, S., Kirby, S., Stakes, D., Mawer, C., 1991. Lithostratigraphic evolution of an in-situ section of oceanic layer 3: evidence from veined rocks, Hole 735B, Southwest Indian Ridge. In: Von Herzen, R.P., Robinson, P.T., et al., Proc. ODP, Sci. Results. Vol. 118, College Station, TX (Ocean Drilling Program), pp. 439–540.

Dick, H.J.B., Natland, J.H., Alt, J.C., Bach, W., Bideau, D., Gee, J.S., Haggas, S., Hertogen, J.G.H., Hirh, G., Holm, P.M., Ildefonse, B., Iturrino, G.J., John, B.E., Kelley, D.S., Kikawa, E., Kingdon, A., LeRoux, P.J., Maeda, J., Meyer, P.S., Miller, J.D., Naslund, H.R., Niu, Y., Robinson, P.T., Snow, J., Stephen, R.A., Trimby, P.W., Worm, H.U., Yoshinobu, A., 2000. A long in-situ section of the lower ocean crust: results of ODP Leg 176 drilling at the Southwest Indian Ridge. Earth Planet. Sci. Lett. 179, 31–51.

Drury, M.J., Hyndman, R.D., 1979. The electrical resistivity of oceanic basalts. J. Geophys. Res. 84, 4537–4546.

Einaudi, F., Pezard, P.A., Cochemé, J.J., Coulon, C., Laverne, C., Godard, M., 2000. Petrography, geochemistry, and physical properties of a continuous extrusive section from the Hilti massif, Semail ophiolite. Submitted for publication.

Fisher, R.L., Sclater, J.G., 1983. Tectonic evolution of the Southwest Indian Ocean since the mid-Cretaceous: plate motions and stability of the pole of Antarctica/Africa for at least 80 Myr. Geophys. J. R. Astron. Soc. 73, 553–576.

Goldberg, D., 1997. The role of downhole measurements in marine geology and geophysics. Rev. Geophys. 35, 315–342.

Guéguen, Y., Palciauskas, V., 1992. Introduction à la physique des roches. Hermann, Paris (299pp.).

Hirth, G., Ildefonse, B., John, B.E., Trimby, P.W., Yoshinobu, A., 2000. Structural evolution of a slow-spreading ridge. Submitted for publication.

Ildefonse, B., Pezard, P., Wilcock, W.S.D., Toomey, D.R., Constable, S., Mainprice, D., 2000. Seismic anisotropy of peridotites and gabbros from the Oman ophiolite (GEOman Experiment), Nice, EGS 2000.

Ildefonse, B., Valsardieu, B., Pezard, P., Mainprice, D., Garrido, C.J., 1999. Petrophysics and anisotropy of gabbros and peridotites from the Oman ophiolite. In: Leiss, B., Ullemeyer, K., Weber, K. (Eds.), Textures and Physical Properties of Rocks. Göttinger Arbeiten zur Geologie und paläontologieGeologische Institute, Universität Göttingen, pp. 73–74.

Iturrino, G.J., Christensen, N.I., Kirby, S., Salisbury, M.H., 1991. Seismic velocities and elastic properties of oceanic gabbroic rocks from Hole 735B. In: Von Herzen, R.P., Robinson, P.T., et al., Proc. ODP, Sci. Results. Vol. 118, College Station, TX (Ocean Drilling Program), pp. 227–244.

Iturrino, G.J., Miller, D.J., Christensen, N.I., 1996. Velocity behavior of lower crustal and upper mantle rocks from a fast-spreading ridge at Hess Deep. In: Mevel, C., Gillis, K., Allan, J.F., et al., Proc. ODP, Sci. Results. Vol. 147, pp. 417–440.

Iturrino, G.J., Ildefonse, B., Boitnott, G., 2000. Velocity structure of the lower oceanic crust: results from ODP hole 735B, Atlantis II Fracture Zone. In: Natland, J., Dick, H.J.B., Miller, J., et al. Submitted for publication.

Kan, R., Sen, P.N., 1987. Electreolytic conduction in periodic arrays of insulators with charges. J. Chem. Phys. 86, 5748–5756.

Karson, J.A., Cannat, M., Miller, Elthon, D.J., D.E., 1997. Proc. ODP, Sci. Results. Vol. 153, College Station, TX (Ocean Drilling Program).

Katsube, T.J., Hume, J.P., 1987. Permeability determination in crystalline rocks by standard geophysical logs. Geophysics 52, 342–352.

Lamoureux, G., Ildefonse, B., Mainprice, D., 1999. Modelling the seismic properties of fast-spreading ridge crustal LVZ: insights from Oman gabbro textures. Tectonophysics 312, 283–301.

MacLeod, C.J., et al., 1998. Geological mapping of slow-spread lower ocean crust: a deep-towed video and wireline rock drilling survey of Atlantis Bank (ODP site 735. SW Indian Ridge). Interridge News 7, 39–43.

Mainprice, D., 1997. Modelling the anisotropic seismic properties of partially molten rocks found at mid-ocean ridges. Tectonophysics 279, 161–179.

Mével, C., Gillis, K.M., Allan, J.F., Meyer, P.S.E., 1996. Proc. ODP, Sci. Results. Vol. 147, College Station, TX (Ocean Drilling Program).

Moos, D., Zoback, M.D., 1990. Utilization of observations of well bore failure to constrain the orientation and magnitude of crustal stresses; application to continental, Deep Sea Drilling Project, and Ocean Drilling Program boreholes. J. Geophys. Res. 95, 9305–9325.

Natland, J.H., Meyer, P.S., Dick, and Bloomer, H.J.B., S.H., 1991. Magmatic oxides and sulfides in gabbroic rocks from Hole 735B and the later development of the liquid line of descent. In: Von Herzen, R.P., Robinson, P.T., et al. Proc. ODP, Sci. Results. Vol. 118, College Station, TX (Ocean Drilling Program), pp. 75–111.

Olhoeft, G.R., 1981. Electrical properties of rocks. In: Touloukian, Y.S., Judd, W.R., Roy, R.F. (Eds.). Physical Properties of Rocks and Minerals. McGraw-Hill, New York, pp. 257–330.

Pape, H., Riepe, L., Schopper, J.R., 1985. Petrophysical detection of microfissures in granite. Trans. SPWLA, 26th Ann. Log. Symp., Paper P.

Pezard, P.A., 1990. Electrical properties of Mid-Ocean Ridge basalt and implications for the structure of the upper oceanic crust in Hole 504B. J. Geophys. Res. 95, 9237–9264.

Pezard, P.A. et al., 1999. Physical properties of granite, with application to nuclear waste storage in subsurface. In: Leiss, B., Ullemeyer, K., Weber, K. (Eds.), Textures and Physical Properties of Rocks. Göttinger Arbeiten zur Geologie und paläontologieGeologische Institute, Universität Göttingen, pp. 149–151.

Pezard, P.A., Howard, J.J., Goldberg, D., 1991. Electrical conduction in oceanic gabbros, Hole 735B, Southwest Indian Ridge. In: Von Herzen, R., Robinson, P.T., et al., Proc. ODP, Sci. Results. Vol. 118, College Station, TX (Ocean Drilling Program), pp. 323–331.

Pezard, P.A., Ito, H., Hermitte, D., Revil, A., 2000. Electrical properties and alteration of granodiorites from the Hirabayashi hole, Japan. USGS open file report 00-129, Proc. Int. Workshop on the Nojima Fault core and borehole data analysis. H. Iko, K. Fujimoto, H Tanaka, D. Lockner (Eds), pp. 255–262.

Pezard, P.A., Luthi, S.M., 1988. Borehole electrical images in the basement of the Cajon Pass Scientific Drillhole, California; fracture identification and tectonic implications. Geophys. Res. Lett. 15, 1017–1020.

Revil, A., Cathles, L.M., Losh, S., Nunn, J.A., 1998. Electrical conductivity in shaly sands with geophysical applications. J. Geophys. Res. 103, 23925–23936.

Revil, A., Glover, P.W.J., 1997. Theory of ionic surface electrical conduction in porous media. Phys. Rev. B 55, 1757–1773.

Revil, A., Glover, P.W.J., 1998. Nature of surface electrical conductivity in natural sands, sandstones, and clays. Geophys. Res. Lett. 25, 691–694.

Shipboard Scientific party, 1999a. Leg 176 Summary. In: Dick, H.J.B., Natland, J.H., Miller, D.J., et al., Proc. ODP, Init. Repts. Vol. 176, College Station, TX (Ocean Drilling Program), pp. 1–70.

Shipboard Scientific party, 1999b. Site 735. In: Dick, H.J.B., Natland, J.H., Miller, D.J., et al., Proc. ODP, Init. Repts. Vol. 176, pp. 1–314 (CD-ROM). Available from: Ocean Drilling Program, Texas A&M University, College Station, TX 77845-9547, USA.

Shipboard Scientific party, 1999c. Explanatory notes. In: Dick, H.J.B., Natland, J.H., Miller, D.J., et al., Proc. ODP, Init. Repts. Vol. 176, pp. 1–42 (CD-ROM). Available from: Ocean Drilling Program, Texas A&M University, College Station, TX 77845-9547, USA

Stakes, D., Mével, C., Cannat, M., Chaput, T., 1991. Metamorphic stratigraphy of Hole 735B. In: Von Herzen, R.P., Robinson, P.T., et al., Proc. ODP, Sci. Results. Vol. 118, College Station, TX (Ocean Drilling Program), pp. 153–180.

Swift, S.A., Hoskins, H., Stephen, R.A., 1991. Seismic stratigraphy in a transverse ridge, Atlantis II Fracture Zone. In: Von Herzen, R.P., Robinson, P.T., et al., Proc. ODP, Sci. Results. Vol. 118, College Station, TX (Ocean Drilling Program), pp. 219–226.

The MELT Seismic Team, 1998. The MELT Experiment. Science 280, 1215–1236.

Tucholke, B.E., Lin, J., Kleinrock, M.C., 1998. Megamullions and mullion structure defining oceanic metamorphic core complexes on the mid-Atlantic ridge. J. Geophys. Res. 103, 9857–9866.

Von Herzen, R.P., Robinson, P.T., et al., 1991. Proc. ODP, Sci. Results. Vol. 118, College Station, TX (Ocean Drilling Program).

Walsh, J.B., Brace, W.F., 1984. The effect of pressure on porosity and the transport properties of rocks. J. Geophys. Res. 89, 9425–9431.

Waxman, M.H., Smits, L.J.M., 1968. Electrical conductivities in oil-bearing shaly sands. Soc. Pet. Eng. J. 8, 107–122.